Polymer 255 (2022) 125150

Contents lists available at ScienceDirect

Polymer

journal homepage: www.elsevier.com/locate/polymer

Rheological properties of crosslinked unentangled and entangled Poly (methyl acrylate) nanocomposite networks

Yi Feng, Di Wu, Ruhao Li, Pinar Akcora *

Department of Chemical Engineering & Materials Science, Stevens Institute of Technology, Hoboken, NJ, 07030, USA

ARTICLE INFO

Keywords:
Nanocomposite
Network
Crosslinked

ABSTRACT

This work is designed to explore the effect of entanglements and particle loading on viscoelastic properties of crosslinked polymer nanocomposites. The entangled and unentangled poly(methyl acrylate) composite networks were synthesized and characterized in linear rheology. We found that the elastic moduli and crosslinking degree of entangled composite networks were unaffected with particle loading. For the unentangled composite networks, both elastic moduli and crosslinking degree enhanced with particle loading. The reinforcement factor analyzed with the recovery of modulus after large deformation indicated that entangled composite networks fully recovered their initial moduli, suggesting the high entanglements can sustain large deformation and maintain their initial chain conformation even at high particle loadings. The unentangled networks did not recover their initial storage moduli after large deformation, posing the non-deformability of the highly crosslinked networks.

1. Introduction

Reinforcement in polymer nanocomposites has been extensively investigated to understand the role of dispersion, particle mobility, particle size, chain entanglements, polymer architecture and particle size [1–19]. Particle dynamics and relaxations of bulk and interfacial chains govern viscoelastic properties of polymer nanocomposites [7,12,15,17,20–25]. It is known that particles with comparable sizes to the entanglement tube lengths move slow following the sub-diffusive dynamics [26]. The constraint release of entangled chains allows particle movements in polymer melts. Chains around nanoparticles disentangle and escape from the reptation tube [27]. Moreover, chain bridging and other conformational states around nanoparticles control the particle diffusion because chain dynamics influences the sub-diffusion paths or the hopping length scale of the particles [28].

Nanoparticle type [29], chain architecture [30–33] and polymer coupled particle dynamics [28] are all critical factors determining the mechanical properties and the processability of filled elastomers. This work is designed to answer some of these factors in composite networks which hold topological constraints from crosslink junctions and entanglements around attractive spherical nanoparticles. In a previous study, the nanoparticle diffusion within entangled and unentangled crosslinked networks was studied by coarse-grained molecular dynamic simulations [34]. It was shown that in the entangled network, viscoelastic properties were dominated by topological entanglements between network strands, whereas in the unentangled (permanent) network, properties were solely controlled by chemical crosslink junctions, with strands moving locally in suppressed sub-diffusive mode [34]. These studies indicate that particle dynamics coupled chain relaxations govern the mechanical properties of crosslinked composites. Olsen et al. explored the effect of defects like loops or dangling chains in the crosslinked network on the bulk elasticity through the real elastic network theory (RENT) [35,36]. In addition, the nanoparticle dynamics within crosslinked network has been investigated experimentally by dynamic light scattering [37], X-ray photon correlation spectroscopy [38], fluorescence correlation spectroscopy [39] and single quantum dots tracking techniques for gel systems [40,41].

This work aims to understand mechanical properties of chemically crosslinked composite networks with different state of entanglements around attractive particles. The unentangled and entangled poly(methyl acrylate) (PMA) crosslinked composites and particle-free crosslinked homopolymer were prepared and tested in linear rheology experiments. The unentangled (permanent) networks were generated by crosslinking the short chains. The crosslinker was added to the growing polymers at different times to attain different strand lengths. Topological constraints of entanglements and reinforcement attributed to the addition of

* Corresponding author.. Castle Point on Hudson, Stevens Institute of Technology, Department of Chemical Engineering & Materials Science, McLean Hall 415, Hoboken, NJ, 07030, USA.
E-mail address: pakcora@stevens.edu (P. Akcora).

https://doi.org/10.1016/j.polymer.2022.125150
Received 3 April 2022; Received in revised form 6 July 2022; Accepted 8 July 2022
Available online 12 July 2022

particles are discussed with the plateau moduli of composite and particle-free networks. Our results show that increasing particle loading enhanced the reinforcement in the unentangled (permanent) networks but had no effect in the entangled composite networks. The modulus recovery measured after large deformation depicted the dynamic differences between different networks. The unentangled networks did not recover their initial storage moduli after large deformation. However, chains fully recovered their initial modulus after deforming the entangled networks, indicating that particles did not disentangle the chains and polymer relaxations remained unperturbed.

2. Experimental

2.1. PMA-SiO_2 composite networks

Methyl acrylate (MA) was polymerized in toluene at 65 °C with the addition of AIBN initiator, silica (SiO_2) nanoparticles of 50-nm in diameter and ethylene glycol dimethacrylate (EGDMA) crosslinker. The total monomer concentration was around 26–34 vol%, depending on the SiO_2 volume in the solution. The mass ratios of EGDMA:MA was 2:100 and 3:100, corresponding to the 1:1100 and 1:730 M ratio, respectively. 4 mg AIBN, 10 mL toluene and SiO_2 solution (1.68–6.72 mL) were added into flask and the gelation was observed in 10–14 h [42]. With the addition of crosslinker and initiator at the same time, the crosslinking occurred spontaneously between short chains. This one-pot synthesis method yielded crosslinking between unentangled PMA chains.

The entangled network composites were prepared in a two-step synthesis, where the crosslinker and SiO_2 nanoparticles were added during polymerization. The solution temperature was quenched after gelation was observed (as seen in Fig. S1). The composite gel was washed with methanol and annealed at 120 °C for 6 days and at 180 °C for 12 h in a vacuum oven. The entangled and unentangled PMA networks are labeled as PMA/E and PMA/U, respectively. Table 1 shows the crosslinker amounts used and reaction times in preparation of different networks. The two reaction methods used are presented in Schema 1. Composite network samples were molded into 8-mm diameter disks at 1-mm thickness by compressing samples between thin Mylar sheets using a CARVER press at 160 °C for 2 h and compressed during cooling. For polymer network, the same procedure was applied without particles. Particle amount in composites was confirmed by Thermogravimetric Analyzer (TGA, Q50 TA Instruments) (Fig. S2). Samples were pre-heated at 150 °C for 20 min then heated up to 580 °C with 20 °C/min heating rate.

2.2. PMA homopolymer synthesis

Methyl acrylate (MA), 4-cyano-4-(phenylcarbonothioylthio) pentanoic acid (CPDB) and 2,2′-azobis(isobutyronitrile) (AIBN) initiator was purchased from Sigma-Aldrich. MA (8 mL), CPDB (7 mg) and AIBN (6 mg) mixture in toluene (10 mL) solution was degassed three times by freeze-pump-thaw and stirred at 90 °C for 16 h. MA monomer was polymerized by reversible addition-fragmentation chain transfer (RAFT) method. The polymer product was purified by washing with methanol and dried at 130 °C in a vacuum oven for 7 days to remove the unreacted monomer. Molecular weight was predicted from the viscosity data (Fig. S3).

Table 1
Unentangled (PMA/2U) and entangled (PMA/2E, PMA/3E) networks prepared for this study.

Sample name	Crosslinker (wt %)	Polymerization time before crosslinking (h)	Particle loading (wt%)
PMA/2U	2	0	0, 10, 20, 40
PMA/2E	2	2	0, 10, 20, 40
PMA/3E	3	3	0, 10, 20, 40

2.3. Crosslinking density measurement

0.2 g of PMA nanocomposite disk sample was soaked in 15 mL chloroform for 7 days. The swollen sample was then gently dried with Kimwipe paper and then weighed. w_1 is the weight of the swollen rubber obtained after subtracting the weight of silica particles. The sample was placed in a vacuum oven at 60 °C for drying until a constant weight was reached. w_3 is the weight of the dry rubber. The amount of solvent in the swollen rubber (w_2) is calculated by subtracting the weight of the dry from the swollen, $w_2 = w_1 - w_3$. The volume fraction of rubber in the gel (v_r) is calculated with the given equation:

$$v_r = \frac{\frac{w_3}{\rho_1}}{\frac{w_3}{\rho_1} + \frac{w_2}{\rho_2}}$$

ρ_1 is the density of dry PMA composite density and ρ_2 is the density of chloroform (1.49 g/cm^3). The crosslinking density, $\frac{1}{M_c}$, is calculated using the Flory-Rehner equation [43]:

$$\frac{1}{M_c} = \frac{-(\ln(1-v_r) + v_r + \chi v_r^2)}{V_0\left(v_r^{\frac{1}{3}} - \frac{v_r}{2}\right)}$$

χ is the polymer solvent interaction parameter for PMA and chloroform ($\chi_{PMA-CHCl_3}$: −0.58) [44], $V_0 = 80$ cm^3/mol is the molar volume of the chloroform.

2.4. Rheology experiments

Rheology measurements were performed by the strain-controlled ARES-G2 rheometer (TA Instruments) equipped with 8-mm parallel plates geometry. The small-amplitude oscillatory shear (SAOS) measurements on samples were conducted at 35 °C, 55 °C, 85 °C, 100 °C, 140 °C and 180 °C. Thermal stability of samples at 180 °C was verified in time sweep experiments performed at 1 rad/s frequency in linear (2% strain) and nonlinear (100% strain) regimes (Fig. S4). Reference temperature in time-temperature superposition (TTS) master curve was 85 °C. Strain sweep tests were conducted at 1 rad/s angular frequency at specified temperature to identify the critical strain (Fig. S5). The shift factors applied in TTS are presented in Fig. S10.

2.5. Small-angle X-ray scattering (SAXS) experiments

SAXS measurements on composites containing 10 and 40 wt% SiO_2 were conducted at the 8-ID-I beamline of the Advanced Photon Source at Argonne National Laboratory. Samples were approximately 0.5-mm in diameter and 2-mm thick and illuminated by coherent X-rays with 11 keV photon energy. SAXS data over the wave vector range 0.0019 nm^{-1} < q < 0.0317 nm^{-1} was collected at 85 °C, following 20 min thermal equilibration. Three different locations on samples were selected to evaluate uniformity and stability of particle dispersion at different temperatures. SAXS data of composite with 20 wt% loading was collected at ambient temperature using Ganesha, SAXSLAB instrument at Columbia University. The equipment has a Cu Kα source (λ = 1.5 Å), a Pilatus 300 K detector with a variable sample-to-detector distance that covers a q range of 0.006–0.03 Å^{-1}.

Particle dispersion of PMA nanocomposites was also characterized using transmission electron microscope (TEM). PMA has a low glass-transition temperature (10 °C); thus, films were cryomicrotomed to 100–200 nm thick sections using a Leica ultramicrotome FC7 with a glass knife at −10 °C and imaged in JEOL-2100Plus TEM operated at 200 keV.

3. Results and discussion

3.1. Rheological behavior of entangled and unentangled PMA networks

The Rouse model describes the dynamics of entangled chains at

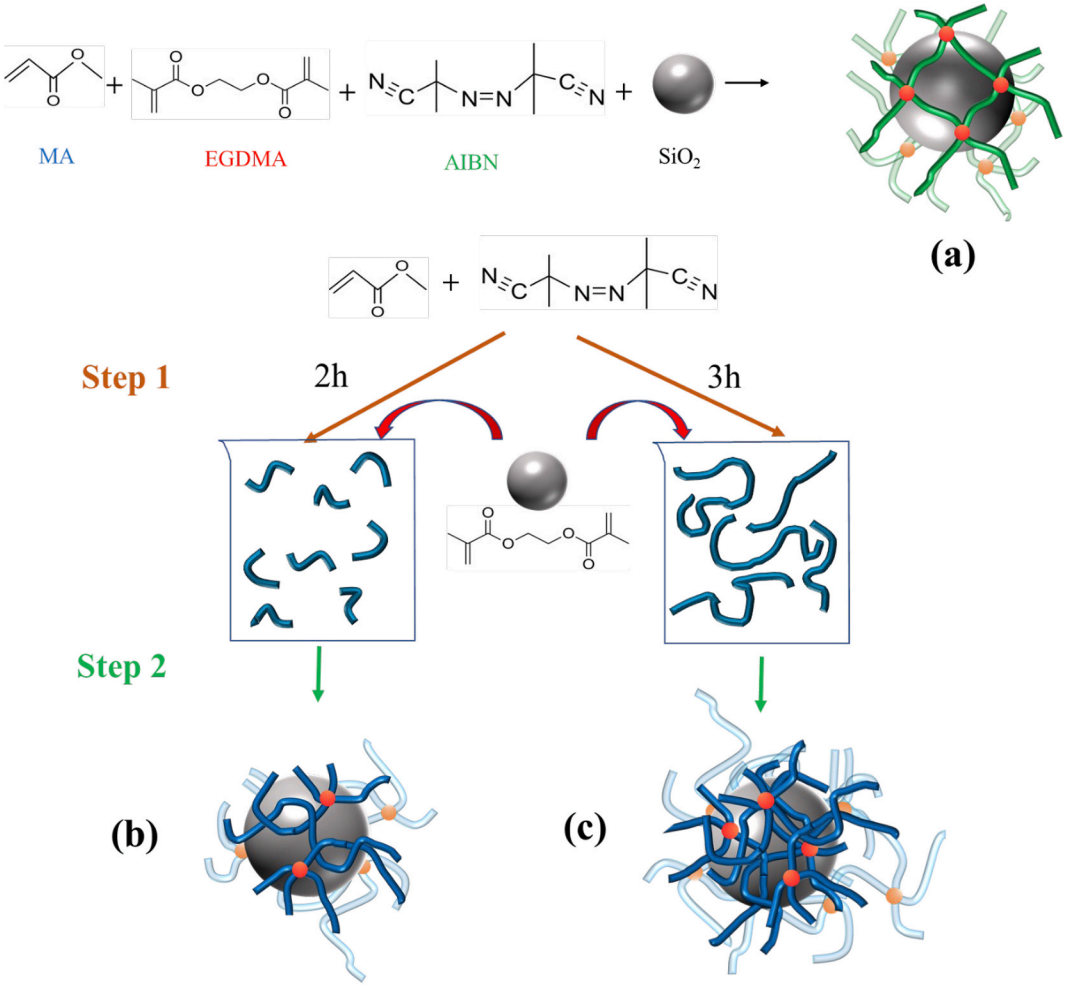

Schema 1. **(a)** One-pot synthesis of unentangled PMA composite network (PMA/2U); **(b, c)** Two-step synthesis of entangled PMA composite networks (PMA/2E and PMA/3E).

intermediate time and length scales. At long times where dynamics of long chains is measured, $\omega < 1/\tau_R$, G' and G'' scales with frequency by $\sim\omega$ [2] and $\sim\omega$ [1], respectively, as shown in Fig. 1a. When polymer chain length is below the entanglement molecular weight, chain dynamics overlaps within $1/\tau_R < \omega < 1/\tau_0$ and both G' and G'' scale with frequency as $\sim\omega^{0.5}$. The overlap of G' and G'' at a wide frequency range (10 [2] $< \omega < 10^4$ rad/s) is observed in our unentangled PMA network (PMA/2U) (Fig. 1b). Frequency independence of storage modulus, $G' \sim \omega^0$, at terminal region for PMA/2U indicates the formation of a permanent network (Fig. 1b) and this overlap region of G' and G'' is a result of the short unentangled chains. A single cross-over point between G' and G'' is observed in the entangled network (PMA/2E) (Fig. 1c). The long-time scale dynamics is dominated by entanglement constraints of long chains and both G' and G'' have frequency dependence of $\sim\omega^{0.2}$. Fig. 1d compares the crosslinked PMA networks with the un-crosslinked PMA homopolymer. Frequency independent moduli of both PMA-2U and PMA/2E samples is a characteristic behavior of gel systems. The long-time relaxations of entangled chains seen in the PMA homopolymer are not seen in crosslinked samples. Storage modulus of the PMA/2E sample is higher than that of the PMA/2U over the intermediate-to-long relaxation times.

The crosslinking density of the unentangled and entangled PMA nanocomposite networks calculated from the swelling experiments indicated that crosslinking density was not affected with particle loading when surrounding chains are entangled (Fig. 2). The crosslinking density increased in the unentangled network with particle loading.

3.2. Particle structures in crosslinked composite networks

Particle aggregations in crosslinked composites were analyzed in SAXS and TEM (Fig. 3a–b and Fig. S6). The wide q-range of the SAXS data collected at 8-ID beamline at Advanced Photon Source (APS) reliably presents the aggregation state of our composites. Two-level unified function given below was fit to SAXS data. This unified approach is the first model that can simultaneously account for exponential scattering and power-law scattering of arbitrary mass, surface-fractal, Porod or diffuse-interfacial scattering [45,46]. It gives accurate values for the power-law exponent (p) and the gyration radius (R_g) of multiple levels of structure.

$$I(q) = \sum_{i=1}^{2}\left(G_i \exp\left(-\frac{q^2R_{gi}^2}{3}\right) + B_i \exp\left(-\frac{q^2R_{g(i+1)}^2}{3}\right)\left(\frac{\left(\operatorname{erf}\left(\frac{qR_{g,i}}{\sqrt{6}}\right)\right)^3}{q}\right)^{P_i}\right)$$

Data of 20% sample was collected from an instrument at Columbia University, so its data is at a narrow q-range and one-level Unified model was used for fitting. Fitting parameters of p_i and $R_{g,i}$ of the two-level Unified function for SAXS data are presented in Table 2. G is the

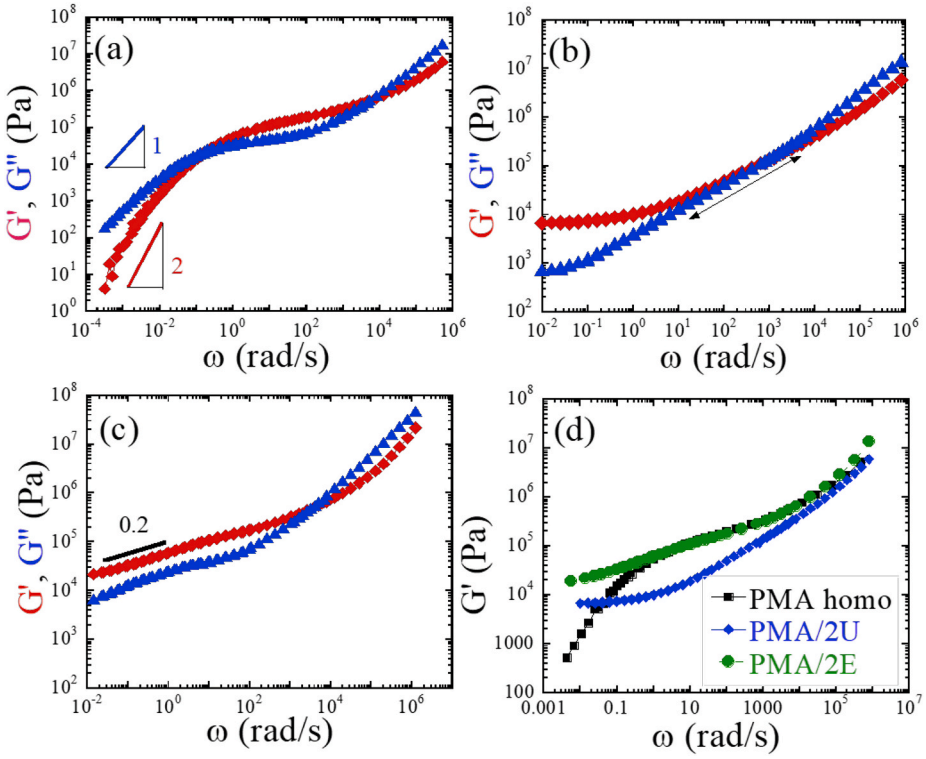

Fig. 1. Linear viscoelastic data of **(a)** neat PMA homopolymer (160 kDa), **(b)** crosslinked unentangled (PMA/2U), **(c)** crosslinked entangled (PMA/2E), **(d)** Storage moduli of PMA homopolymer, PMA/2U and PMA/2E networks.

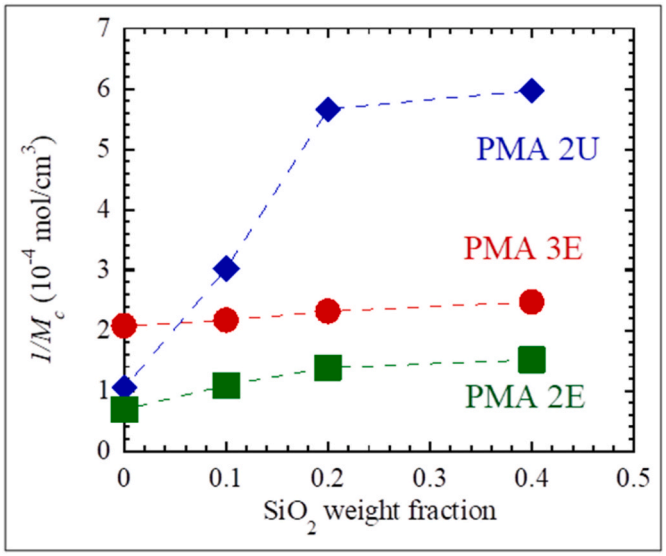

Fig. 2. Crosslinking density ($1/M_c$) of PMA nanocomposite networks at different entanglement states with particle loading. PMA/2U presents the unentangled network; and PMA/3E and PMA/2E represent the entangled network created.

Guinier pre-factor describing the population of a structure; and G_2/G_1 ratios represent the population of structures for R_{g1}, R_{g2}. B is the pre-factor specific to the type of power-law scattering, and p is the power-law exponent describing the fractal shapes. Fractal dimension (p_1) was found to be ~4 for all samples, that was suggested for sharp interphases of particles. As shown in Table 2, the aggregate size (R_2) did not increase with particle loading in any of the networks. PMA/2E sample had similar structure sizes at 10 and 40 wt%. In 3E and 2U samples, structures were smaller at 40% compared to their 10% (Table 2). TEMs in Fig. 3a and **S6** all show aggregated structures. It is important to mention the crosslinked samples are difficult to microtome or cryomicrotome as samples are prone to deform due to their crosslinked states. Therefore, TEM data by itself is insufficient to determine the state of particle dispersions. Interestingly, a similar particle loading effect was observed in the rheology data presented in Fig. 3c. It is apparent that the particle reinforcement in the PMA/2E entangled network was only slightly higher in 40 wt% sample, and the aggregate sizes were also similar in both loadings. In the unentangled composite networks (PMA/2U), however, G' increased significantly at 20 and 40 wt% loadings compared to 10 wt% (Fig. 3d). Simply, the sample with the larger particle structures behaved more reinforced. The reinforcement measured in 2U networks for three particle loadings is related to their high crosslinking density as shown in Fig. 2. We present the linear characteristics of the prepared samples in the following section and then discuss their modulus recovery to deformation to further understand the nature of reinforcement in composite networks and their particle-free crosslinked forms.

The SAOS data of PMA composite (40 wt%) networks are compared with the crosslinked neat homopolymers in Fig. 4a–c. The terminal relaxation time (τ_d) is immeasurable in crosslinked samples. At high frequency region $\omega > 1/\tau_e$, the transition zone between glassy and plateau regions is observed. G_N^o is the storage modulus of the composite at the frequency where tan(δ) is at minimum [47] and is shown for each sample in Fig. S7. The PMA/2E-40% has the higher plateau value of G_N^o at low frequency than the neat one (PMA/2E-0%) (Fig. 4a). G_N^o of the more entangled (PMA/3E-40%) composite network is interestingly similar to that of the neat system (PMA/3E-0%) (Fig. 4b). Higher crosslinking degree reinforces the permanent network (PMA/2U) (Fig. 4c) and its G_N^o is also higher than its neat form. Data for PMA/3E-10 and -20 wt% particle loadings are presented in Fig. S8.

To understand the particle loading effect on moduli of these different networks, we normalized the plateau modulus of the PMA composite network ($G_{N,CN}^o$) by the plateau modulus of the neat PMA network (G_N^o).

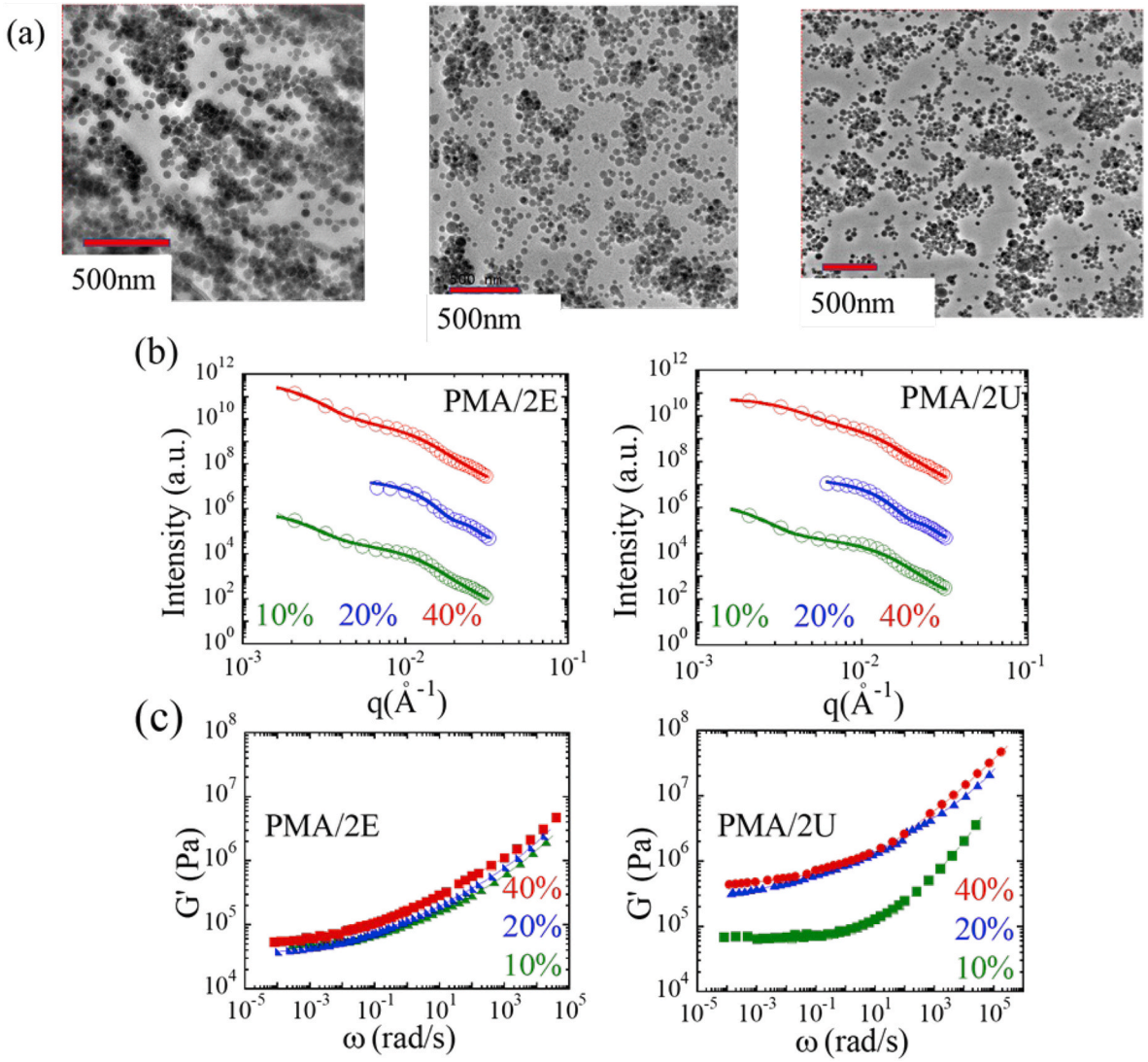

Fig. 3. **(a)** TEM data of PMA/2U (left), PMA/3E (middle) and PMA/2E (right) nanocomposite networks with 40 wt% SiO_2. **(b)** SAXS and **(c)** Small amplitude oscillatory shear (SAOS) data of PMA nanocomposite networks (PMA/2U and PMA/2E) with 10, 20 and 40 wt% SiO_2. The reference temperature is 85 °C. SAXS data of all samples except 20% was collected at 8-ID beamline at APS. SAXS data of 20 wt% sample was collected from SAXS instrument at Columbia University.

Table 2
SAXS data model fitting parameters for all PMA composite networks.

Sample	G_2/G_1	p_1	R_1(Å)	p_2	R_2 (Å)
PMA2E10	37.17	4 ± 0.21	190.6 ± 5.3	4 ± 0.11	965.5 ± 8.2
PMA2E20	–	4 ± 0.15	238.4 ± 8.7	–	–
PMA2E40	80.72	4 ± 0.17	190.6 ± 4.6	4 ± 0.15	955.5 ± 9.3
PMA3E10	65.25	4 ± 0.11	172.5 ± 5.6	3.6 ± 0.12	1106.0 ± 12.3
PMA3E20	–	4 ± 0.18	234.0 ± 6.2	–	–
PMA3E40	10.31	4 ± 0.23	225.5 ± 3.2	4.2 ± 0.18	585 ± 7.3
PMA2U10	46.91	4 ± 0.10	170.4 ± 5.4	4.2 ± 0.21	1056.0 ± 14.1
PMA2U20	–	4 ± 0.13	234.0 ± 6.8	–	–
PMA2U40	10.54	4 ± 0.18	192.5 ± 4.9	4.2 ± 0.23	556.0 ± 7.5

Fig. 4d shows that the normalized plateau modulus increases with particle loading in a permanent network (PMA/2U). For the entangled networks, the normalized G_N^o is not affected by particle loadings at 10–20 wt%. Slight increase of 40 wt% PMA/2E sample is explained by the chain bridging that can yield additional physical networking, and presumably the higher effective crosslink density compared to the lower particle loadings. The plateau modulus value for each polymer nanocomposite and matrix are shown in Fig. S11.

3.3. Crosslinking and particle constraints on modulus recovery

The entanglement state of the two entangled networks and particle agglomerates may influence the modulus recovery when composites are applied large-amplitude oscillatory shear. Linear viscoelastic responses at 2% strain and 1 rad/s frequency were measured during resting times. Linear homopolymers under large strains can fully recover their initial entanglements and storage moduli during resting. The modulus recovery to large strains is critical in demonstrating the effects of entanglement density and desorption/adsorption rate of polymers at interfacial regions of particles [48,49]. The difference in G' before and after large deformation shows the extent of the modulus recovery (ΔG) and it is attributed to the breakdown of particle network and to the possible particle rearrangement under large oscillatory shear [50,51]. Fig. 5a shows the recovery of homopolymer after shear. With the comparison of its composite, we observe how particles influence the chain conformations and relaxations. ΔG is significantly small 0.014 kPa for homopolymer and it fully recovers (ΔG = 0) to the modulus with 40 wt% particles. This is reasonable because terminal relaxation time (τ_d) of PMA 160 kDa is 0.01 s at 180 °C, which explains the quick recovery of PMA 160 kDa nanocomposite to its initial modulus after large deformation. For the neat PMA/2U network, the ΔG is 1.4 kPa which is higher

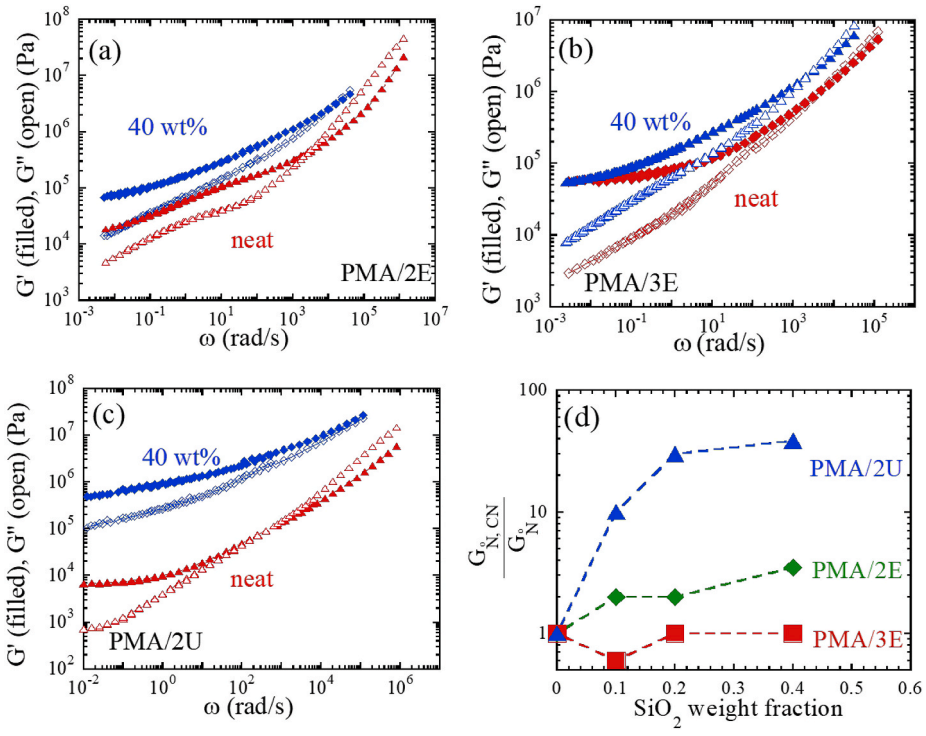

Fig. 4. Comparison of viscoelastic response of neat networks with their composite (40 wt% SiO_2) forms for **(a)** PMA/2E; **(b)** PMA/3E; **(c)** PMA/2U; **(d)** Composite network plateau modulus ($G^o_{N,CN}$) normalized by the pure network plateau modulus (G^o_N) in PMA/2U, PMA/2E and PMA/3E.

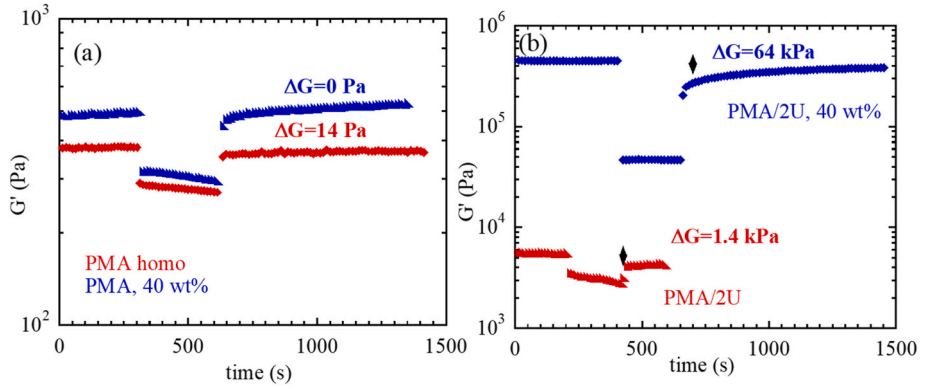

Fig. 5. Time sweep data of **(a)** PMA160 kDa homopolymer and its composite at 40 wt% loading. **(b)** PMA/2U network and its composite 40 wt% loading. The low strain, $\gamma_1 = 2\%$ and large strain amplitudes are $\gamma_2 = 100\%$. Data is collected at 180 °C and 1 rad/s frequency.

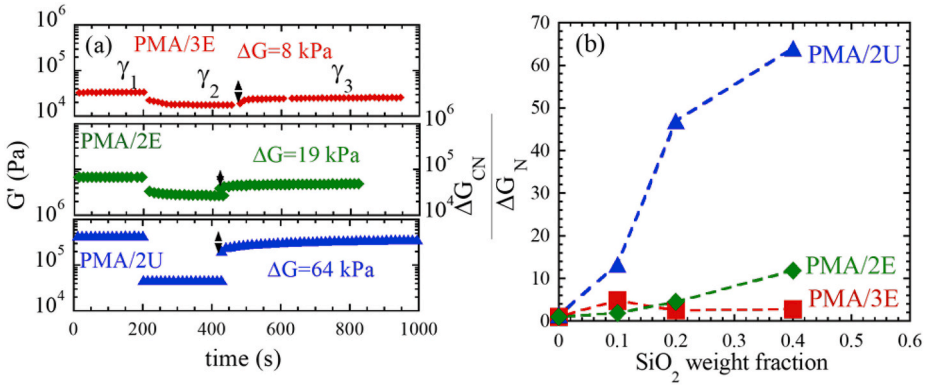

Fig. 6. **(a)** Time sweep data of 40 wt% PMA composite networks at strains $\gamma_1 = 2\%$, $\gamma_2 = 100\%$, $\gamma_3 = 2\%$. **(b)** Modulus recovery difference of composite networks (ΔG_{CN}) normalized by their neat network forms (ΔG_N) for different SiO_2 particle loadings. Data is collected at 180 °C and 1 rad/s frequency.

by a factor of 100 than the homopolymer. Crosslinked chains of PMA/2U cannot relax by chain reptation which was verified with no crossover point of G' and G'' at terminal region in Fig. 1b–c.

Fig. 6a compares storage moduli of 40 wt% composite networks before and after shear at 100% strain during time sweeps. As seen, the unentangled network composite has the largest $\Delta G = 64$ kPa at 40 wt%. Data for other loadings at 10–20 wt% are presented in Fig. S9. To investigate the relative value of ΔG between three different networks, the modulus recovery response of all composites at different loadings are normalized by the modulus of particle-free crosslinked forms in Fig. 6b. We anticipated that particle loading should have high impact on modulus recovery. However, in PMA-3E sample, the recovery modulus was particle independent. The slight modulus recovery increase in PMA-2E shows clear differences between entangled matrices.

4. Conclusions

The entangled and unentangled PMA-SiO_2 composite networks were prepared, and their linear rheological properties were characterized to evaluate the particle addition and entanglement contributions to the overall modulus. The PMA homopolymer, crosslinked PMA network and PMA-SiO_2 composite networks were tested in small-amplitude oscillatory shear experiments, and their plateau moduli and recovery to large deformation are discussed to underpin the particle and entanglement effects on reinforcement. Physical and chemical networks of entangled chains of PMA/2E, PMA/3E samples can recover their initial moduli instantly as measured by small modulus recovery, ΔG. These results suggest that entangled networks can sustain large deformation and nanoparticles do not perturb chain relaxations of the entangled network even at high particle loadings. The reinforcement which enhances with particle loading in the stiff permanent network composites (PMA/2U) was shown to be distorted by deformation. The permanent network deformation and particle size effect will be examined in future studies.

Supplementary data

Photograph of crosslinked PMA composite; TGA data of PMA nanocomposites; viscosity versus shear rate of PMA homopolymer; viscoelastic data during time sweep experiment on PMA homopolymer; strain-sweep data of crosslinked PMA networks; SAXS and TEM data of PMA/3E composites at different particle loadings; tangent loss versus frequency data for PMA/2E and PMA/3E composites; SAOS data of PMA/3E composites; storage modulus measured in time sweep experiments at different strain steps; time-temperature superposition shift factors.

Funding sources

This material is based upon work supported by the National Science Foundation CMMI MEP program under Grant No. 1825250.

CRediT authorship contribution statement

Yi Feng: Conceptualization, Methodology, Validation, Investigation, Writing – original draft, Visualization. **Di Wu:** Methodology, Formal analysis. **Ruhao Li:** Investigation. **Pinar Akcora:** Conceptualization, Writing – review & editing, Supervision, Funding acquisition, Project administration.

Declaration of competing interest

The authors declare that they have no known competing financial interests or personal relationships that could have appeared to influence the work reported in this paper.

Data availability

Data will be made available on request.

Acknowledgements

We thank Prof. Sanat K. Kumar for the SAXS experiments conducted at Columbia University. This research used resources of the Advanced Photon Source, a U.S. Department of Energy (DOE) Office of Science User Facility operated for the DOE Office of Science by Argonne National Laboratory under Contract No. DE-AC02-06CH11357.

Appendix A. Supplementary data

Supplementary data to this article can be found online at https://doi.org/10.1016/j.polymer.2022.125150.

References

[1] B.M. Yavitt, D. Salatto, Y. Zhou, Z. Huang, M. Endoh, L. Wiegart, V. Bocharova, A. E. Ribbe, A.P. Sokolov, K.S. Schweizer, T. Koga, Collective nanoparticle dynamics associated with bridging network formation in model polymer nanocomposites, ACS Nano 15 (7) (2021) 11501–11513.
[2] M. Tress, S. Ge, K. Xing, P.F. Cao, T. Saito, A.C. Genix, A.P. Sokolov, Turning rubber into a glass: mechanical reinforcement by microphase separation, ACS Macro Lett. 10 (2) (2021) 197–202.
[3] J.F. Moll, P. Akcora, A. Rungta, S. Gong, R.H. Colby, B.C. Benicewicz, S.K. Kumar, Mechanical reinforcement in polymer melts filled with polymer grafted nanoparticles, Macromolecules 44 (18) (2011) 7473–7477.
[4] E. Senses, A. Isherwood, P. Akcora, Reversible thermal stiffening in polymer nanocomposites, ACS Appl. Mater. Interfaces 7 (27) (2015) 14682–14689.
[5] S. Yang, P. Akcora, Deformation of chemically heterogeneous interfacial layers of polymer nanocomposites, ACS Macro Lett. 8 (12) (2019) 1635–1641.
[6] P. Akcora, S.K. Kumar, J. Moll, S. Lewis, L.S. Schadler, Y. Li, B.C. Benicewicz, A. Sandy, S. Narayanan, J. Ilavsky, P. Thiyagarajan, R.H. Colby, J.F. Douglas, "Gel-like" mechanical reinforcement in polymer nanocomposite melts, Macromolecules 43 (2) (2010) 1003–1010.
[7] S. Merabia, P. Sotta, D.R. Long, A microscopic model for the reinforcement and the nonlinear behavior of filled elastomers and thermoplastic elastomers (Payne and Mullins Effects), Macromolecules 41 (21) (2008) 8252–8266.
[8] C.C. Lin, S. Gam, J.S. Meth, N. Clarke, K.I. Winey, R.J. Composto, Do attractive polymer-nanoparticle interactions retard polymer diffusion in nanocomposites? Macromolecules 46 (11) (2013) 4502–4509.
[9] D. Zhao, S. Ge, E. Senses, P. Akcora, J. Jestin, S.K. Kumar, Role of filler shape and connectivity on the viscoelastic behavior in polymer nanocomposites, Macromolecules 48 (15) (2015) 5433–5438.
[10] R.B. Bogoslovov, C.M. Roland, A.R. Ellis, A.M. Randall, C.G. Robertson, Effect of silica nanoparticles on the local segmental dynamics in poly(vinyl acetate), Macromolecules 41 (4) (2008) 1289–1296.
[11] D. Wu, Y. Feng, R. Li, R. Ozisik, P. Akcora, Entanglement density and particle dynamics in rigid interfacial layers of polymer nanocomposites, J. Appl. Phys. 130 (6) (2021).
[12] S. Liu, E. Senses, Y. Jiao, S. Narayanan, P. Akcora, Structure and entanglement factors on dynamics of polymer-grafted nanoparticles, ACS Macro Lett. 5 (5) (2016) 569–573.
[13] E. Senses, M. Tyagi, M. Pasco, A. Faraone, Dynamics of architecturally engineered all-polymer nanocomposites, ACS Nano 12 (11) (2018) 10807–10816.
[14] E. Senses, S. Darvishi, M.S. Tyagi, M.S. Tyagi, A. Faraone, Entangled polymer dynamics in attractive nanocomposite melts, Macromolecules 53 (12) (2020) 4982–4989.
[15] E.J. Bailey, K.I. Winey, Dynamics of polymer segments, polymer chains, and nanoparticles in polymer nanocomposite melts: a review, Prog. Polym. Sci. (2020) 105.
[16] E.J. Bailey, P.J. Griffin, R.J. Composto, K.I. Winey, Multiscale dynamics of small, attractive nanoparticles and entangled polymers in polymer nanocomposites, Macromolecules 52 (5) (2019) 2181–2188.
[17] J. Yang, M. Melton, R. Sun, W. Yang, S. Cheng, Decoupling the polymer dynamics and the nanoparticle network dynamics of polymer nanocomposites through dielectric spectroscopy and rheology, Macromolecules 53 (1) (2019) 302–311.
[18] G.P. Baeza, C. Dessi, S. Costanzo, D. Zhao, S. Gong, A. Alegria, R.H. Colby, M. Rubinstein, D. Vlassopoulos, S.K. Kumar, Network dynamics in nanofilled polymers, Nat. Commun. 7 (2016).
[19] S.K. Kumar, B.C. Benicewicz, R.A. Vaia, K.I.J.M. Winey, 50th anniversary perspective: are polymer nanocomposites practical for applications? Macromolecules 50 (3) (2017) 714–731.
[20] L.-H. Cai, S. Panyukov, M.J.M. Rubinstein, Mobility of nonsticky nanoparticles in polymer liquids, Macromolecules 44 (19) (2011) 7853–7863.
[21] K.K. Senanayake, E.A. Fakhrabadi, M.W. Liberatore, A.J.M. Mukhopadhyay, Diffusion of nanoparticles in entangled poly (vinyl alcohol) solutions and gels, Macromolecules 52 (3) (2019) 787–795.

[22] A. Karatrantos, R.J. Composto, K.I. Winey, M. Kröger, N. Clarke, Modeling of entangled polymer diffusion in melts and nanocomposites: a review, Polymers 11 (5) (2019).
[23] A. Karatrantos, R.J. Composto, K.I. Winey, N. Clarke, Polymer and spherical nanoparticle diffusion in nanocomposites, J. Chem. Phys. 146 (20) (2017).
[24] E. Senses, A. Faraone, P. Akcora, Microscopic chain motion in polymer nanocomposites with dynamically asymmetric interphases, Sci. Rep. 6 (2016), 29326.
[25] S. Cheng, V. Bocharova, A. Belianinov, S. Xiong, A. Kisliuk, S. Somnath, A.P. Holt, O.S. Ovchinnikova, S. Jesse, H. Martin, T. Etampawala, M. Dadmun, A.P. Sokolov, Unraveling the mechanism of nanoscale mechanical reinforcement in glassy polymer nanocomposites, Nano Lett. 16 (6) (2016) 3630–3637.
[26] H. Guo, G. Bourret, R.B. Lennox, M. Sutton, J.L. Harden, R. Leheny, Entanglement-controlled subdiffusion of nanoparticles within concentrated polymer solutions, Phys. Rev. Lett. 109 (5) (2012), 055901.
[27] R. Mangal, S. Srivastava, L.A. Archer, Phase stability and dynamics of entangled polymer-nanoparticle composites, Nat. Commun. 6 (2015) 1–9.
[28] Z.E. Dell, K.S. Schweizer, Theory of localization and activated hopping of nanoparticles in cross-linked networks and entangled polymer melts, Macromolecules 47 (1) (2014) 405–414.
[29] M.S. Reid, T.C. Stimpson, E. Niinivaara, M. Villalobos, E.D.J.I. Cranston, E. C. Research, Comparing Soft Semicrystalline Polymer Nanocomposites Reinforced with Cellulose Nanocrystals and Fumed Silica, vol. 57, 2018, pp. 220–230, 1.
[30] S.J.M. Panyukov, Loops in polymer networks 52 (11) (2019) 4145–4153.
[31] B.J. Anderson, C.F. Zukoski, Rheology and microstructure of entangled polymer nanocomposite melts, Macromolecules 42 (21) (2009) 8370–8384.
[32] B.J. Anderson, C.F. Zukoski, Rheology and microstructure of an unentangled polymer nanocomposite melt, Macromolecules 41 (23) (2008) 9326–9334.
[33] L. Zhao, Y.-G. Li, C. Zhong, Integral Equation Theory Study on the Phase Separation in Star Polymer Nanocomposite Melts, J. Chem. Phys. 127 (15) (2007) 1544909, 154909.
[34] Y. Chen, R. Ma, X. Qian, R. Zhang, X. Huang, H. Xu, M. Zhou, J. Liu, Nanoparticle mobility within permanently cross-linked polymer networks, Macromolecules 53 (11) (2020) 4172–4184.
[35] M. Zhong, R. Wang, K. Kawamoto, B.D. Olsen, J.A. Johnson, Quantifying the impact of molecular defects on polymer network elasticity, Science 353 (6305) (2016) 1264–1268.
[36] R. Wang, J.A. Johnson, B.D. Olsen, Odd–even effect of junction functionality on the topology and elasticity of polymer networks, Macromolecules 50 (6) (2017) 2556–2564.
[37] S. Rose, A. Marcellan, D. Hourdet, C. Creton, T. Narita, Dynamics of hybrid polyacrylamide hydrogels containing silica nanoparticles studied by dynamic light scattering, Macromolecules 46 (11) (2013) 4567–4574.
[38] J. Reina, R. Bansil, C. Koňák, Dynamics of probe particles in polymer solutions and gels, Polymer 31 (6) (1990) 1038–1044.
[39] S. Walta, F. Di Lorenzo, K. Ma, U. Wiesner, W. Richtering, S. Seiffert, Diffusion of rigid nanoparticles in crowded polymer-network hydrogels: dominance of segmental density over crosslinking density, Colloid Polym. Sci. 295 (8) (2017) 1371–1381.
[40] C.H. Lee, A.J. Crosby, T. Emrick, R.C. Hayward, Characterization of heterogeneous polyacrylamide hydrogels by tracking of single quantum dots, Macromolecules 47 (2) (2014) 741–749.
[41] E. Parrish, M.A. Caporizzo, R.J. Composto, Network confinement and heterogeneity slows nanoparticle diffusion in polymer gels, J. Chem. Phys. 146 (20) (2017), 203318.
[42] R. Scherf, L.S. Müller, D. Grosch, E.G. Hübner, W. Oppermann, Investigation on the homogeneity of PMMA gels synthesized via RAFT polymerization, Polymer 58 (2015) 36–42.
[43] P.J. Flory, Principles of Polymer Chemistry, Cornell University Press, 1953.
[44] N. Schuld, B. Wolf, Polymer-solvent interaction parameters, Polymer handbook 4 (1999).
[45] G. Beaucage, In Combined Small-Angle Scattering for Characterization of Hierarchically Structured Polymer Systems over Nano-To-Micron Meter: Part II Theory, 2012.
[46] G. Beaucage, Approximations leading to a unified exponential/power-law approach to small-angle scattering, J. Appl. Crystallogr. 28 (6) (1995) 717–728.
[47] C. Liu, J. He, E. Van Ruymbeke, R. Keunings, C. Bailly, Evaluation of different methods for the determination of the plateau modulus and the entanglement molecular weight, Polymer 47 (13) (2006) 4461–4479.
[48] D. Roy, C. Roland, Reentanglement kinetics in polyisobutylene, Macromolecules 46 (23) (2013) 9403–9408.
[49] N. Li, Q. Zhang, Q. Yang, Y. Huang, X. Liao, W. Zhao, The dependence time of melting behavior on rheological aspects of disentangled polymer melt: a route to the heterogeneous melt, J. Polym. Res. 22 (4) (2015) 1–7.
[50] A.-J. Zhu, S. Sternstein, Nonlinear viscoelasticity of nanofilled polymers: interfaces, chain statistics and properties recovery kinetics, Compos. Sci. Technol. 63 (8) (2003) 1113–1126.
[51] Z. Zhu, T. Thompson, S.-Q. Wang, E.D. von Meerwall, A. Halasa, Investigating linear and nonlinear viscoelastic behavior using model silica-particle-filled polybutadiene, Macromolecules 38 (21) (2005) 8816–8824.